AFRL-RX-WP-JA-2018-0315

POST-DEPOSITION ANNEALING EFFECTS ON FERROMAGNETIC COFEB THIN FILMS (POSTPRINT)

Ryan A. O'Dell, Adam B. Phillips, Daniel G. Georgiev, and Michael J. Heben

University of Toledo

John G. Jones and Gail J. Brown

AFRL/RX

27 April 2018
Interim Report

(STINFO COPY)

AIR FORCE RESEARCH LABORATORY
MATERIALS AND MANUFACTURING DIRECTORATE
WRIGHT-PATTERSON AIR FORCE BASE, OH 45433-7750
AIR FORCE MATERIEL COMMAND
UNITED STATES AIR FORCE

REPORT DOCUMENTATION PAGE

Form Approved
OMB No. 0704-0188

1. REPORT DATE *(DD-MM-YY)*	2. REPORT TYPE	3. DATES COVERED *(From - To)*
27 April 2018	Interim	8 September 2016 – 27 March 2018

4. TITLE AND SUBTITLE
SUBSTRATE HEATING EFFECTS ON STRUCTURAL AND FERROMAGNETIC RESONANCE PROPERTIES OF CO40FE40B20 THIN FILMS (PREPRINT)

5a. CONTRACT NUMBER
FA8650-16-D-5408-0001

5b. GRANT NUMBER

5c. PROGRAM ELEMENT NUMBER
62102F

6. AUTHOR(S)
1) Ryan A. O'Dell, Adam B. Phillips, Daniel G. Georgiev, and Michael J. Heben – University of Toledo
2) John G. Jones and Gail J. Brown - AFRL/RX

5d. PROJECT NUMBER
4348

5e. TASK NUMBER 0001

5f. WORK UNIT NUMBER
X0YN

7. PERFORMING ORGANIZATION NAME(S) AND ADDRESS(ES)
1) University of Toledo
2801 W. Bancroft
Toledo, OH 43606-3390
2) AFRL/RX
Wright-Patterson AFB
Dayton, OH 45433

8. PERFORMING ORGANIZATION REPORT NUMBER

9. SPONSORING/MONITORING AGENCY NAME(S) AND ADDRESS(ES)
Air Force Research Laboratory
Materials and Manufacturing Directorate
Wright-Patterson Air Force Base, OH 45433-7750
Air Force Materiel Command
United States Air Force

10. SPONSORING/MONITORING AGENCY ACRONYM(S)
AFRL/RXAN

11. SPONSORING/MONITORING AGENCY REPORT NUMBER(S)
AFRL-RX-WP-JA-2018-0315

12. DISTRIBUTION/AVAILABILITY STATEMENT
DISTRIBUTION STATEMENT A. Approved for public release: distribution is unlimited.

13. SUPPLEMENTARY NOTES
PA Case Number: 88ABW-2018-2205; Clearance Date: 27 Apr 2018. This document contains color. Journal article published in IEEE Transactions on Magnetics, Vol. 54, No. 10, 10 Oct 2018. © 2018 IEEE. The U.S. Government is joint author of the work and has the right to use, modify, reproduce, release, perform, display, or disclose the work.
The final publication is available at https:// DOI: 10.1109/TMAG.2018.2845394

14. ABSTRACT ***(Maximum 200 words)***
We investigate the role of annealing Co40Fe40B20 at different temperatures and how it affects the crystallinity and the ferromagnetic resonance (FMR) behavior. The onset of crystallization was shown to occur after annealing in nitrogen at 370 °C for 1 h. The crystallization peak of the post-annealed Co40Fe40B20 was matched to the analysis of (110) Co7Fe3, due to secondary phase segregation. Magnetic force microscopy images show a pattern of magnetization ripples in the magnetic phase images for samples up to 250 °C. The grain size of the Co7Fe3 (110) was shown to increase from 20 to 56 nm when annealed above 370 °C to 600 °C. The segregated Co7Fe3 causes scattering of the FMR linewidth, which shifts the resonance peak location, broadens peak-to-peak linewidth, and causes an additional resonance peak to appear close to the uniform resonance of the amorphous phase. Annealing above 500 °C leads to a complete phase change to Co7Fe3, which changes the FMR spectra back to a single resonance peak, shifted to lower fields with broader peak-to-peak linewidth of ~71.2 (kA/m).

15. SUBJECT TERMS
Annealing, atomic force microscopy, ferromagnetic resonance (FMR), X-ray diffraction (XRD)

16. SECURITY CLASSIFICATION OF:			17. LIMITATION OF ABSTRACT:	18. NUMBER OF PAGES	19a. NAME OF RESPONSIBLE PERSON (Monitor)
a. REPORT	b. ABSTRACT	c. THIS PAGE			Joseph Burns
Unclassified	Unclassified	Unclassified	SAR	9	19b. TELEPHONE NUMBER *(Include Area Code)* (937) 255-9594

Post-Deposition Annealing Effects on Ferromagnetic CoFeB Thin Films

Ryan A. O'Dell[1,2], Adam B. Phillips[3], Daniel G. Georgiev[1], John G. Jones[2], Gail J. Brown[2], and Michael J. Heben[3]

[1]Department of Electrical Engineering and Computer Science, The University of Toledo, Toledo, OH 43606 USA
[2]Materials and Manufacturing Directorate, Air Force Research Laboratory, Dayton, OH 45433 USA
[3]Department of Physics and Astronomy, The University of Toledo, Toledo, OH 43606 USA

We investigate the role of annealing $Co_{40}Fe_{40}B_{20}$ at different temperatures and how it affects the crystallinity and the ferromagnetic resonance (FMR) behavior. The onset of crystallization was shown to occur after annealing in nitrogen at 370 °C for 1 h. The crystallization peak of the post-annealed $Co_{40}Fe_{40}B_{20}$ was matched to the analysis of (110) Co_7Fe_3, due to secondary phase segregation. Magnetic force microscopy images show a pattern of magnetization ripples in the magnetic phase images for samples upto 250 °C. The grain size of the Co_7Fe_3 (110) was shown to increase from 20 to 56 nm when annealed above 370 °C to 600 °C. The segregated Co_7Fe_3 causes scattering of the FMR linewidth, which shifts the resonance peak location, broadens peak-to-peak linewidth, and causes an additional resonance peak to appear close to the uniform resonance of the amorphous phase. Annealing above 500 °C leads to a complete phase change to Co_7Fe_3, which changes the FMR spectra back to a single resonance peak, shifted to lower fields with broader peak-to-peak linewidth of ∼71.2 (kA/m).

Index Terms— **Annealing, atomic force microscopy, ferromagnetic resonance (FMR), X-ray diffraction (XRD).**

I. Introduction

COMBINING boron with $Co_{1-x}Fe_x$ binary alloys leads to the formation of amorphous or nanocrystalline ferromagnetic alloys [1], [2]. As boron is added to the binary alloy, the resistivity increases and the saturation magnetization decreases [3]. The grain size reduces with the increase of boron concentration, showing grain sizes of 20 nm at (2 at % B) and reducing to ∼10 nm at (17 at % B) based on analyzing the X-ray diffraction (XRD) peaks using the Scherrer formula [4]. The amorphous alloy of $Co_{40}Fe_{40}B_{20}$ has soft ferromagnetic properties where thin films with thickness of about 2 nm are used in high-frequency spintronic applications as a free layer in magnetic tunnel junctions (MTJs) [5], [6]. These materials are often annealed to improve the (100) body center cubic (BCC) crystalline structure [7]–[9].

For a high-frequency operation, magnetic parameters such as Gilbert damping (α), effective magnetization (M_{eff}), and spectroscopic splitting g-factor are important. At a thickness of 10 nm, as-deposited (ASD) $Co_{40}Fe_{40}B_{20}$ has been reported to have a damping value of $\alpha = 0.004$ [10]. At a thickness of ∼100 nm, damping values for ASD $Co_{40}Fe_{40}B_{20}$ varied from 0.05–0.013 by varying sputtering pressure from 0.1 to 0.4 Pa [11]. The effective magnetization for $Co_{40}Fe_{40}B_{20}$ thin films with thicknesses of 10, 78, and 100 nm were 1436, 1280, and 1396 (kA/m), respectively [10], [12].

As $Co_{40}Fe_{40}B_{20}$ is annealed above 300 °C, partial crystallization occurs and the magnetization properties begin to change. In some publications, the crystallization of $Co_{40}Fe_{40}B_{20}$ leads to the loss of low-frequency (6 GHz) ferromagnetic resonances (FMRs) and increased FMR linewidth [13]. The use of differential scanning calorimetry showed the crystallization transition temperature to be 373 °C for $Co_{40}Fe_{40}B_{20}$ samples on glass substrates [14]. According to phase diagrams, $Co_{40}Fe_{40}B_{20}$ has a solid solution for a BCC structure at 900 °C and face centered cubic (FCC) at 1000 °C [15]. In some cases, $Co_{40}Fe_{40}B_{20}$ crystalizes into a BCC CoFe phase in both MTJ and single-layer structures as a result of boron migration [12].

Amorphous ferromagnetic alloys that use boron or other metalloid elements have been shown to segregate into multiple phases when heated to critical temperatures close to the crystallization point [16], [17]. This results in an inhomogeneous-mixed-phased ferromagnetic layer composed of a nanocrystalline phase and an amorphous phase. The magnetization changes, as a function of annealing temperature, are lacking for independent thin films of $Co_{40}Fe_{40}B_{20}$. FMR is a non-invasive way to study magnetization changes, in particular, those of Gilbert damping and linewidth relaxation. It is a form of microwave spectroscopy where a ferromagnetic sample absorbs electromagnetic radiation with wavelengths typically between 1 mm and 10 cm.

FMR probes the uniform mode or spin wave with wave vector $\mathbf{k} = 0$. Spin waves have properties similar to those of photons and phonons and are often referred to as magnons [18], [19]. The microwave absorption of the ferromagnetic alloy at different frequencies can be fit to equations to determine the damping, magnetization, and other material parameters. Collisions between particles of different kinds such as phonons, conduction electrons, and magnons play a crucial role in the relaxation processes [20]–[22]. Shifts in the resonance position and broadening can occur through the

Manuscript received February 8, 2018; revised March 27, 2018; accepted May 22, 2018. Date of publication August 17, 2018; date of current version September 18, 2018. Corresponding author: R. A. O'Dell (e-mail: rodell@ashland.edu).

Color versions of one or more of the figures in this paper are available online at http://ieeexplore.ieee.org.

Digital Object Identifier 10.1109/TMAG.2018.2845394

two-magnon scattering [23]. It has been shown that when two distinct magnetic phases are present, multiple resonances can occur related to the individual magnetic phases, which have different g-factors and magnetization values [24].

Magnetization properties such as those related to $Co_{40}Fe_{40}B_{20}$ changes from an amorphous phase to a crystalline phase are still not well understood. The material properties that contribute to an increased damping and loss of low-frequency resonance are not well documented. Thermal annealing of the $Co_{40}Fe_{40}B_{20}$ may result in partial crystallization when it is close to known crystallization temperatures. This can result in a mixture of multiple phases, which would lead to additional scattering events, which in turn would increase damping values. In this work, we investigate the structural properties such as crystallinity, grain size, and surface roughness of the ferromagnetic $Co_{40}Fe_{40}B_{20}$ alloy deposited on a Si wafer as a function of the annealing temperature. In addition, we investigate the first-derivative peak-to-peak FMR linewidth, Gilbert damping, and effective magnetization as a function of the annealing temperature. We show how thermal annealing leads to secondary phase segregation and multiple FMRs in a single-layer thin film.

II. Materials and Methods

A thin film was sputtered from a 2″ $Co_{40}Fe_{40}B_{20}$ target supplied by ACI ALLOYS, onto a 2 in, and p-type Si (100) wafer at 20 °C an Ar pressure of 0.67 Pa using a system with a base pressure $\leq 1.33 \times 10^{-4}$ Pa. X-ray reflectivity and ellipsometry were used on the ASD sample after growth to determine that the thickness was 78.2 nm. After deposition, samples were diced from the 2″ wafer and annealed from 100 °C to 600 °C for 60 min in a tube furnace with slowly flowing N_2.

The samples were characterized by XRD using a Bruker D2 Phaser with a 1-D Lynxeye detector; by vibrating-sample magnetometry (VSM) using Quantum Designs VersaLab; and by FMR using a 5403 GMW electromagnet with a strip transmission line waveguide while applying a microwave-frequency signal from an HP 5200b sweep oscillator. XRD peak and phase analysis were done using a Bruker software DIFFRAC.EVA.

Ferromagnetic thin films were placed onto a strip transmission waveguide where a fixed microwave frequency f (GHz) was applied. An in-plane external magnetic field $H_{\rm dc}$ is incremented from 0 to 2650 Oe while the fixed frequency is applied. The first derivative FMR absorption signal (dP/dH) is recorded and a derivative Lorentzian function is used to determine the resonance position and peak-to-peak linewidth. At each microwave frequency, the derivative absorption signal measured at an external field $H_{\rm dc}$ is fit to

$$\frac{dP}{dH} = \frac{\left(\left(\frac{\Delta H}{2}\right)^2 - (H_{\rm dc} - H_r)^2\right)\sin\phi - (2\Delta H(H_{\rm dc} - H_r))\cos\phi}{\left[\left(\frac{\Delta H}{2}\right)^2 + (H_{\rm dc} - H_r)^2\right]^2} \tag{1}$$

where ΔH is the full width at half max (FWHM) of the Lorentzian absorption, H_r is the FMR center, and ϕ relates the absorptive and dispersive components of the equation. The FWHM is related to the peak-to-peak linewidth by $\Delta H_{pp} = \Delta H/\sqrt{3}$.

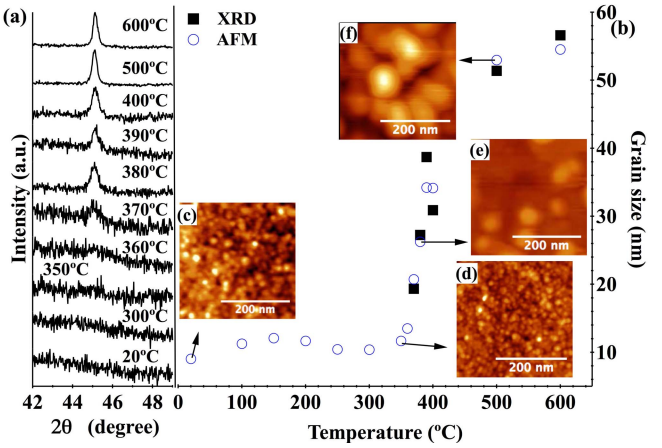

Fig. 1. Crystallographic and surface analysis of annealed $Co_{40}Fe_{40}B_{20}$ thin films on Si (100). (a) XRD from ASD-600 °C. (b) Grain size of XRD and AFM data. (c)–(f) AFM topography images of 20 °C, 350 °C, 380 °C, and 500 °C films.

After each fixed frequency f (GHz) measurement, the fit values of H_r are used to determine the g-factor and effective magnetization $M_{\rm eff}$ by fitting to the in-plane Kittel equation [25]

$$f\,(\text{GHz}) = \frac{g\mu_0\mu_B}{h}\sqrt{(H_{\rm Res})(H_{\rm Res} + M_{\rm eff})} \tag{2}$$

where g is the spectroscopic splitting factor [26], μ_B is the Bohr magneton, μ_0 is the permeability of free space, h is Planck's constant, and $H_{\rm Res} = H_r$ is the FMR resonance center field position. The Gilbert damping parameter, α, defined in the Landau–Lifshitz–Gilbert equation [27], and inhomogeneous linewidth broadening $\Delta H_{pp,0}$ were determined by fitting the FMR peak-to-peak linewidth to [28]

$$\Delta H_{pp} = \Delta H_{pp,0} + \frac{2\alpha h}{\sqrt{3} g\mu_B\mu_0} f. \tag{3}$$

Scanning probe microscopy images were done using an Asylum Cypher S Atomic Force Microscope (AFM). Magnetic force microscopy (MFM) images were taken with a cobalt-coated magnetic tip that is lifted up to 100 nm in the noncontact mode to collect MFM image.

III. Results

A. Effects of Annealing on Film Crystallinity

In Fig. 1, we show the XRD pattern of the post-annealed $Co_{40}Fe_{40}B_{20}$ thin films along with the corresponding grain size analysis.

As the XRD data shows Fig. 1(a), $Co_{40}Fe_{40}B_{20}$ thin films were amorphous in room temperature until the annealing temperature reached 370 °C. After annealing to 370 °C, a broad diffraction peak can be observed around 45°, which indicates that a small amount of crystallization is taking place. Phase analysis of the post-annealed 370 °C XRD peak at 45.1120° was matched to the primary (110) peak of the Co_7Fe_3 alloy [29]. This is a cubic crystal structure with a space group of Pm-3m (221).

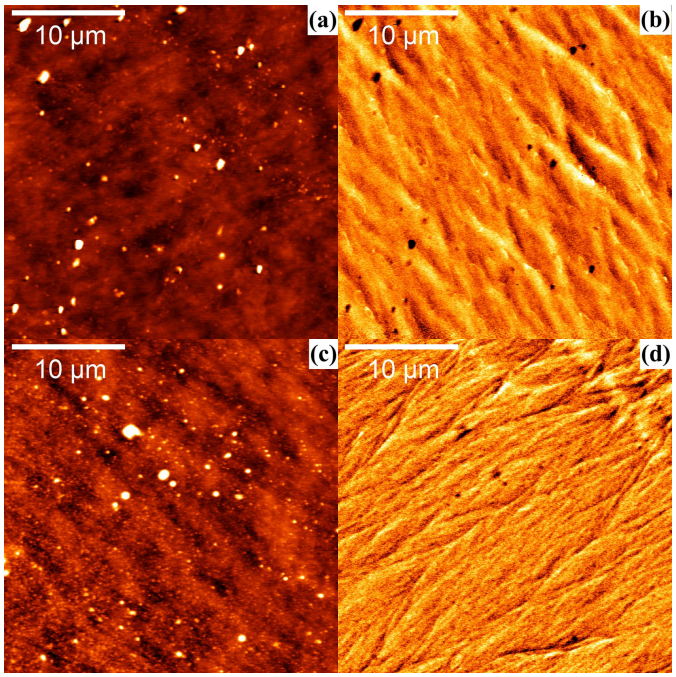

Fig. 2. MFM surface and magnetic domain images. (a) and (b) ASD topography and MFM phase. (c) and (d) 250 °C topography and MFM phase.

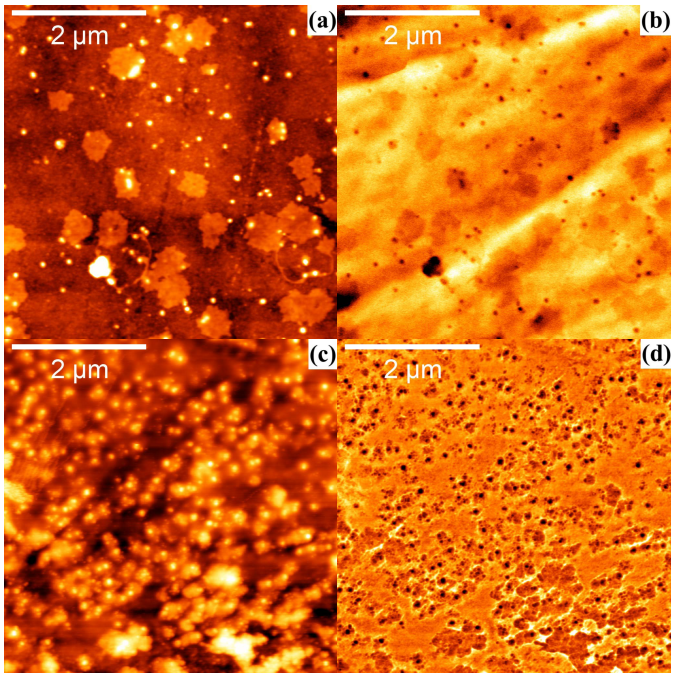

Fig. 3. MFM surface and magnetic domain images. (a) and (b) 350 °C topography and MFM phase. (c) and (d) 400 °C topography and MFM phase.

As the annealing temperature is increased to 600 °C, this peak becomes more defined and its FWHM is reduced. The intensity of the diffraction peak increases showing that the crystallization of this particular orientation is increasing in volume. A singular XRD peak at 45.1120° appeared throughout all crystalized samples where the Scherrer equation [30], [31] was used to determine grain size of the (110) Co_7Fe_3 peak. Phase diagrams for ternary alloy of iron, cobalt, and boron show a solid solution for a BCC $(CoFe)_2B$ alloy at 900 °C. However, the post-annealed $Co_{40}Fe_{40}B_{20}$ alloy crystallized into a completely different material with an FCC structure. The boron may be similar to an impurity, which diffuses from the alloy upon annealing.

In Fig. 1(b), the grain size analysis from XRD and AFM measurements shows that the grain size increases with annealing temperature. The ASD sample exhibited a grain size of 9 nm determined from AFM measurements shown in Fig. 1(c). The grain size gradually grows to 11.5 nm after annealing to 350 °C, and slightly after crystallization, the grain size increases to 26 nm at 380 °C as shown in Fig. 1(d) and (e). At 500 °C, the grain size has increased to 51.4 nm determined from the XRD analysis, which is in close agreement to the AFM measurement of 52.9 nm shown in Fig. 1(f).

The topography of the ASD sample measured with an MFM tip showed small aggregates on the sample surface as shown in Fig. 2(a). The magnetic domain structure of the ASD sample showed large wavelike in-plane longitudinal domain structures in the remnant state (zero field, $H_{dc} = 0$) as shown in Fig. 2(b). This non-uniform wavelike fluctuation is known as magnetization ripple [32]. This structure was observed for samples from room temperature up to 250 °C. This occurs when ferromagnetic materials contain random local anisotropies from inhomogeneities. The dark spots in the MFM phase shown in Fig. 2(b) and (d) are likely small inhomogeneities such as secondary phase materials or spike domains. According to Cullity and Graham [33], regions of differing spontaneous magnetizations are magnetic inclusions, which act as hindrance to domain-wall motion. The magnetic inclusions can be voids or second-phased material in metallic alloys that are either nonmagnetic or magnetic.

The magnetic inclusions appear to be segregated material based on the topography images shown in Fig. 2(a) and (c). These inclusions are magnetic; however, according to the XRD analysis, there is no crystallization at the annealing temperature of 250 °C.

As the annealing temperature is increased to 350 °C, the topography began to show large clusters of material forming on the surface as shown in Fig. 3(a). At 400 °C, these clusters are more prominent on the surface as shown in Fig. 3(c). The magnetization ripple is slightly present at 350 °C; however, the segregated material differs in magnetization leading to spots in the MFM image as shown in Fig. 3(b). The wavelike magnetization pattern is lost after annealing to 400 °C and all that remains are clustered regions of differing magnetization. The clusters are believed to be the regions of Co_7Fe_3 material, which are segregating from the amorphous material. It will be shown that changes in the crystallinity and grain size influence both the VSM and FMR properties of the sample.

B. Vibrating Sample Magnetometry

In Fig. 4, we use an in-plane magnetizing field to measure magnetization as a function of the applied field in hysteresis loops of post-annealed ferromagnetic thin films.

In order to normalize hysteresis loops, each magnetic induction curve is divided by the saturation magnetization (M/M_s).

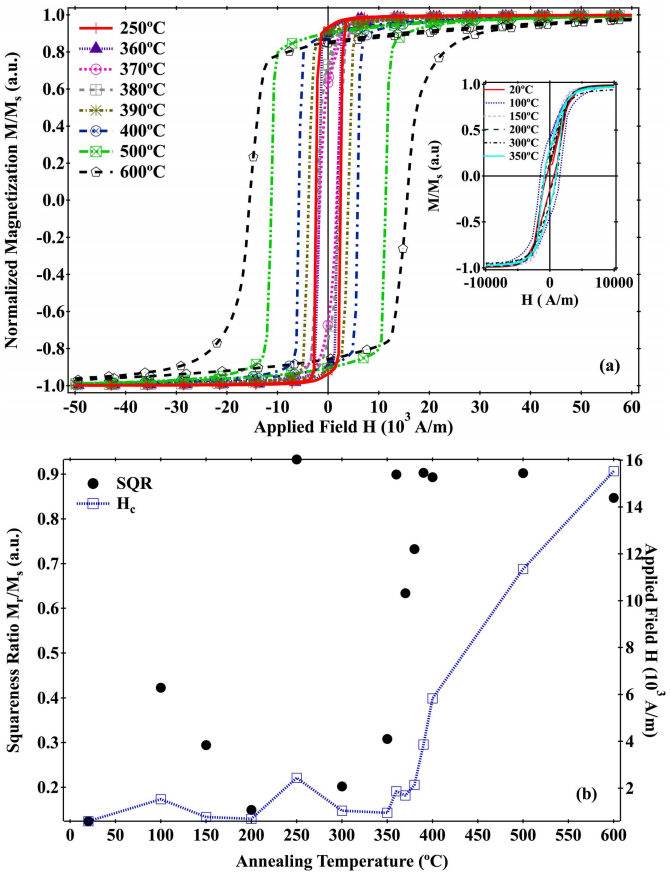

Fig. 4. In-plane VSM data for post-annealed $Co_{40}Fe_{40}B_{20}$ thin films. (a) Normalized hysteresis loops 360 °C–600 °C. Inset: 20 °C–350 °C. (b) SQR (M_r/M_s) and coercivity H_c with annealing temperature.

Amorphous thin films (RT–350 °C) have hysteresis loops with small areas and reach saturation quickly as shown in Fig. 4(a) (inset). The amorphous phase exhibits magnetically soft ferromagnetic behavior with low coercivity H_c = 589–1000 (A/m) as shown in Fig. 4(a) and (b). After the application of a saturating magnetic field, samples have a residual or remanent magnetization M_r at zero external field strength $H_{\rm dc} = 0$.

At room temperature, the squareness ratio (SQR) is small with $(M_r/M_s) = 0.124$, which increases to 0.31 after annealing to 350 °C. The sample holds very little magnetization when the field is reduced to zero, which means the particle size is small. Upon crystallization at 370 °C, the coercivity increases to 1687 A/m and the squareness increases to 0.63 where SQR values over 0.5 can indicate larger grain sizes. At 500 °C, the coercivity increases to 11.3 (kA/m) with an SQR of 0.9 as shown in Fig. 4(b). It can be seen that the hysteresis loop area has greatly increased at 500 °C in comparison with the area of the ASD sample as shown in Fig. 4(a).

C. Ferromagnetic Resonance

The uniform mode or spin wave with wave vector $\mathbf{k} = 0$ of a ferromagnetic thin film is probed using FMR by applying a microwave frequency perpendicular to a static magnetic field across the thin-film plane. When the microwave pump frequency matches the precession of the magnetization in

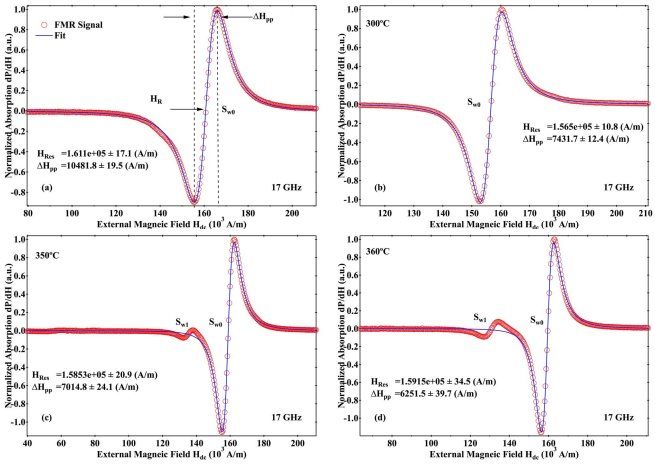

Fig. 5. First derivative FMR absorption curves for post-annealed $Co_{40}Fe_{40}B_{20}$ thin films. (a) ASD. (b) 300 °C. (c) 350 °C. (d) 360 °C.

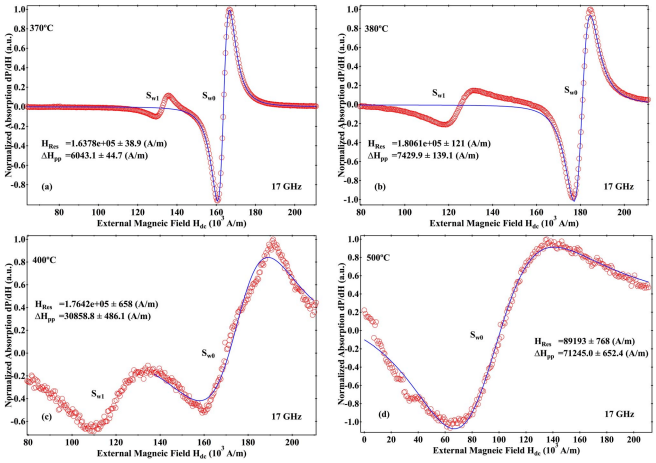

Fig. 6. First derivative FMR absorption curves for post-annealed $Co_{40}Fe_{40}B_{20}$ thin films. (a) 370 °C. (b) 380 °C. (c) 400 °C. (d) 500 °C.

the material, the sample undergoes FMR. In Fig. 5, the first derivative FMR absorption data (dP/dH) were fit to (1) where the linewidth shape is considered Lorentzian.

The ASD sample at room temperature and annealed samples up to 300 °C only exhibit a singular resonance peak S_{w0} as shown in Fig. 5(a) and (b). At 300 °C and 350 °C, the annealed samples in Fig. 5(b) and (c) show a reduced peak-to-peak linewidth of ∼7.4 and 7.0 (kA/m) as compared to the room temperature 10.5 (kA/m) at 17 GHz. The resonance location is slightly shifted to lower magnetic field strengths of 156.5 and 158.5 (kA/m) compared to 161.1 (kA/m) at 17 GHz. At 350 °C and 360 °C, there exists a secondary resonance peak S_{w1} at lower field strength than the primary uniform resonance.

As the annealing temperature is increased from 370 °C to 400 °C, there continues to be multiple resonance peaks present as shown in Fig. 6(a)–(c). The primary resonance peak $H_{\rm Res}$ at 370 °C is centered at 163.7 (kA/m) with at linewidth of ∼6.0 (kA/m), which is shifted to a higher field with a lower linewidth than the as-grown RT sample. At 380 °C, in Fig. 6(b), the resonance position continues to move to higher fields 180.6 (kA/m) and linewidth increases to 7.4 (kA/m). The linewidth continues to broaden for annealed samples at 400 °C

and 500 °C increasing to 30.9 and 71.2 (kA/m), respectively, as shown in Fig. 6(c) and (d). At 500 °C, the secondary resonance peak disappears and a single broad resonance peak shifted down to 89.1 (kA/m) is all that remains.

The secondary resonances observed in this FMR experiment only occurred for samples annealed above 350 °C, which is very close to the first observed crystallization peak at 370 °C. If two magnetic phases are present, they can be coupled together via the exchange interaction. When magnetic inhomogeneities are present in the material, the uniform procession excited during resonance with wave vector $\mathbf{k} = 0$ can couple with spin waves having a wave vector $\mathbf{k} \neq 0$ [22], [34], [35]. This can result in a singular resonance peak, which can cause shifts in the resonance peak position. The separation into multiple resonances is a result of crystallite growth of the secondary phase Co_7Fe_3 reaching a grain size significant enough to where it can support its own resonance [16]. This has occurred around 12 nm as indicated in the grain size analysis in Fig. 1(b) for the annealed 350 °C sample. This value is in agreement with the 10–20 nm ranges, which can support a standing spin-wave mode. Energy from the uniform mode can be dissipated into non-uniform modes, which leads to larger linewidth.

The additional resonance peaks were only observed above 8 GHz from post-annealed samples from 350 °C to 400 °C. The coupling between Co_7Fe_3 and $Co_{40}Fe_{40}B_{20}$ causes shifts in the resonance position and increases inhomogeneous linewidth broadening to the peak-to-peak linewidth. The resonance position data was fit to (2) using a spectroscopic splitting g-factor of 2.16. The g-factor for CoFe alloys varies between 2.09 and 2.15 [36], [37] and CoFeB-based materials varies between 2 and 2.22 [38]–[41].

In Fig. 7, we show the first derivative FMR positions H_{res} and peak-to-peak linewidth ΔH_{pp} data fit to (1) for post-annealed samples from 2 to 18 GHz. The resonance position increases in field strength as the microwave frequency is increased following an in-plane Kittel equation, which is fit by dashed lines as shown in Fig. 7(a). Shifts in the resonance position to lower field strengths at the same frequency correspond to an increase in effective magnetization.

The effective magnetization values in Fig. 7(b) are determined from the Kittel fits in Fig. 7(a). The effective magnetization M_{eff}, at room temperature was fit by (2) and found to be 1076 (kA/m) and increased, to 1159 (kA/m) at 250 °C as shown in Fig. 7(c). The magnetization decreases to 1108 (kA/m) at 300 °C and 1061 (kA/m) at 370 °C. The effective magnetization values found in our experiment are comparable to the 1280 (kA/m) reported for a 78 nm thick thin film [12]. The effective magnetization values for annealed films at 500 °C and 600 °C could not be determined from FMR due to the limited data points that could be collected to fit (2).

The room temperature data for the first derivative peak-to-peak ferromagnetic linewidth ΔH_{pp} increases from 3.7 to 10.4 (kA/m) with an increased microwave pump frequency shown in Fig. 7(c). The magnetization loses energy to the thermal bath of the system through scattering from phonons and impurities, where the Gilbert damping parameter (α) fit in (3) is a fitting parameter to describe this behavior

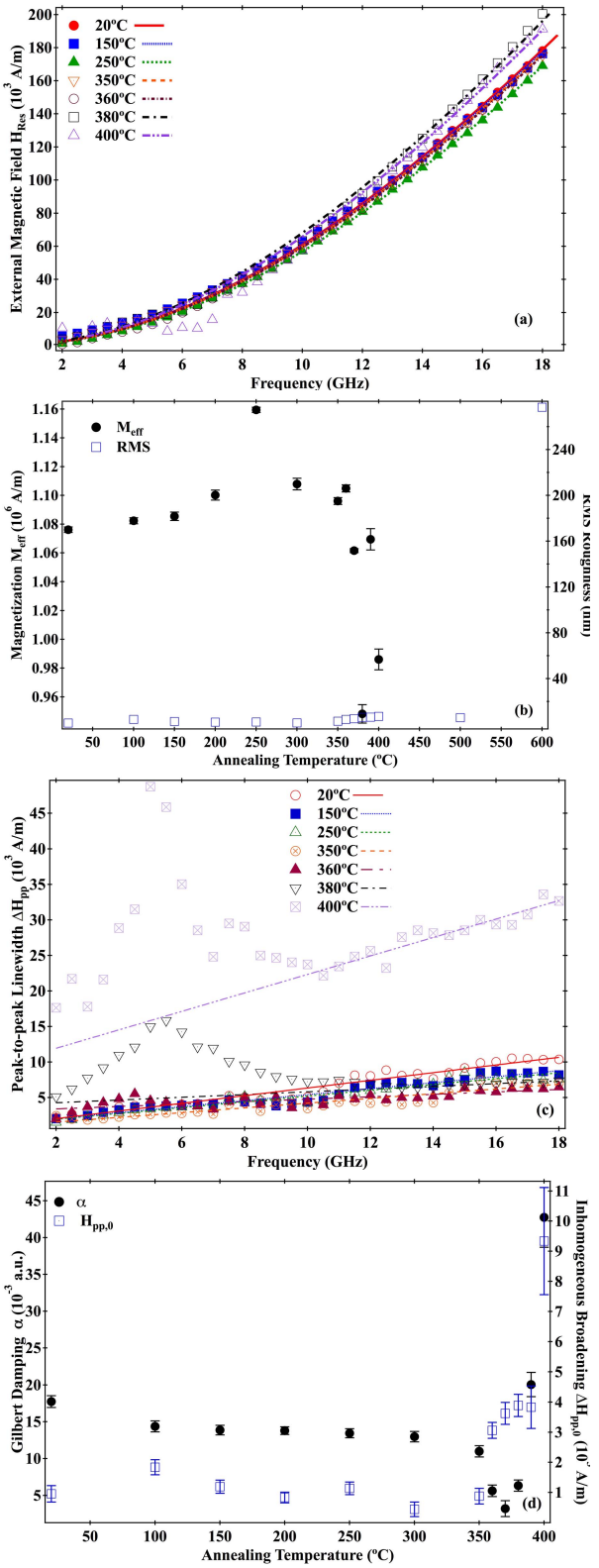

Fig. 7. Extrapolated FMR data from fits to absorption curves. (a) FMR position and Kittel fits. (b) Effective magnetization and root mean square roughness from AFM. (c) Peak-to-peak linewidth where lines are fits to (3). (d) Gilbert damping and inhomogeneous peak-to-peak broadening.

with frequency. The samples show a reduction in peak-to-peak linewidth with an increased annealing temperature up to 350 °C as shown in Fig. 7(c). The ASD Gilbert damping

parameter is 0.017 and reduces to 0.011 after annealing to 350 °C as shown in Fig. 7(d).

The use of thermal annealing may relive strain in the film, which may be the cause in the reduction on both overall linewidth and damping. After annealing to 360 °C, the linewidth of the lower frequency resonances between 2 and 6 GHz began to increase above the previously annealed samples, whereas the linewidth of the 8–18 GHz resonances are still below those of the as-grown sample as shown in Fig. 7(c). At the onset of crystallization at 370 °C, the damping is ∼0.003 and increases to 0.04 at 400 °C. The linewidth is increasing continuously as the material crystalizes into the hard ferromagnetic Co_7Fe_3 alloy.

The overall peak-to-peak linewidth has contributions that are both intrinsic and extrinsic. The inhomogeneous linewidth broadening parameter provides a fit contribution to the amount of extrinsic linewidth broadening that may be present in the sample by possible magnetocrystalline and non-uniform strain, which is fit by (3). The FMR technique is very sensitive to surface properties because the microwave only penetrates a limited depth from the surface due to the skin effect. Phase segregation from thermal annealing increases the surface roughness from 1.2 nm for the ASD sample to ∼6 nm after annealing to 500 °C as shown in Fig. 7(c).

The inhomogeneous linewidth broadening parameter varies as the sample is annealed being 1.8 (kA/m) at room temperature, 1.2 (kA/m) at 150 °C, and 1.1 (kA/m) at 250 °C until 300 °C where it reaches the lowest point at 440 (A/m). The broadening continuously increases after 300 °C reaching 3.6 (kA/m) at 370 °C. The increase in coercivity and the field required to saturate the sample leads to broadening of low-frequency linewidth and inhomogeneous linewidth broadening.

IV. Conclusion

We have investigated the effect of thermal annealing on the damping constant and crystallinity of 78 nm thick $Co_{40}Fe_{40}B_{20}$ thin films. The damping value decreases until the alloy crystalizes at 370 °C into a secondary-phased FFC (110) Co_7Fe_3material. Broadening of a uniform mode FMR linewidth occurs due to scattering from secondary-phased ferromagnetic material. The inhomogeneous-mixed-phased ferromagnetic sample exhibits multiple resonance peaks in the first derivative FMR spectra when the grain size of the secondary phase reaches a critical limit.

Acknowledgment

This work was supported by The Dayton Area Graduate Studies Institute and The Air Force Research Laboratory (AFRL) through the Cooperative Agreement FA8650-12-2-7248, "AFRL Collaborative Student-Faculty Research Program." This work was supported by AFRL RX: Materials and Manufacturing under research topic RX15-3.

References

[1] R. C. O'Handley, "Physics of ferromagnetic amorphous alloys," *J. Appl. Phys.*, vol. 62, pp. R15–R49, Jul. 1987.

[2] H. Kronmüller, M. Fähnle, M. Domann, H. Grimm, R. Grimm, and B. Gröger, "Magnetic properties of amorphous ferromagnetic alloys," *J. Magn. Magn. Mater.*, vol. 13, pp. 53–70, Sep. 1979.

[3] I. Kim, J. Kim, K. H. Kim, and M. Yamaguchi, "Effects of boron contents on magnetic properties of Fe-Co-B thin films," *IEEE Trans. Magn.*, vol. 40, no. 4, pp. 2706–2708, Jul. 2004.

[4] H. Karamon, T. Masumoto, and Y. Makino, "Magnetic and electrical properties of Fe-B-N amorphous films (invited)," *J. Appl. Phys.*, vol. 57, pp. 3527–3532, Apr. 1985.

[5] S. Ikeda *et al.*, "A perpendicular-anisotropy CoFeB-MgO magnetic tunnel junction," *Nature Mater.*, vol. 9, no. 9, pp. 721–724, Jul. 2010.

[6] S. Ikeda *et al.*, "Tunnel magnetoresistance of 604% at 300K by suppression of Ta diffusion in CoFeB/MgO/CoFeB pseudo-spin-valves annealed at high temperature," *Appl. Phys. Lett.*, vol. 93, p. 082508, Aug. 2008.

[7] J. Hayakawaa, S. Ikeda, Y. M. Lee, F. Matsukura, and H. Ohno, "Effect of high annealing temperature on giant tunnel magnetoresistance ratio of CoFeB/MgO/CoFeB magnetic tunnel junctions," *Appl. Phys. Lett.*, vol. 89, p. 232510, Dec. 2006.

[8] J. J. Cha, J. C. Read, R. A. Buhrman, and D. A. Müller, "Spatially resolved electron energy-loss spectroscopy of electron-beam grown and sputtered CoFeB/MgO/CoFeB magnetic tunnel junctions," *Appl. Phys. Lett.*, vol. 91, p. 062516, Aug. 2007.

[9] J. W. Cao, Y. Liu, Y. Ren, F. L. Wei, and P. P. Freitas, "Effect of annealing temperature on formation of superparamagnetism in CoFeB/MgO/CoFeB magnetic tunnel junctions," *Appl. Surf. Sci.*, vol. 314, pp. 443–446, Sep. 2014.

[10] X. Liu, W. Zhang, M. Carter, and G. Xiao, "Ferromagnetic resonance and damping properties of CoFeB thin films as free layers in MgO-based magnetic tunnel junctions," *J. Appl. Phys.*, vol. 110, p. 033910, Aug. 2011.

[11] F. Xu, Q. Huang, Z. Liao, S. Li, and C. K. Ong, "Tuning of magnetization dynamics in sputtered CoFeB thin film by gas pressure," *J. Appl. Phys.*, vol. 111, p. 07A304, Apr. 2012.

[12] A. Conca *et al.*, "Annealing influence on the Gilbert damping parameter and the exchange constant of CoFeB thin films," *Appl. Phys. Lett.*, vol. 104, p. 182407, May 2014.

[13] Y. Zhang *et al.*, "Study and tailoring spin dynamic properties of CoFeB during rapid thermal annealing," *Appl. Phys. Lett.*, vol. 98, p. 042506, Jan. 2011.

[14] J.-Y. Tseng, Y.-T. Chen, Z. G. Chang, C. W. Wu, and L. C. Yang, "Crystallization behavior and thermal analysis of CoFeB thin films," *J. Nanomater.*, vol. 2015, Apr. 2015, Art. no. 371894.

[15] V. Raghavan, "B-Co-Fe (boron-cobalt-iron)," *J. Phase Equilibria Diffusion*, vol. 33, pp. 392–394, Oct. 2012.

[16] D. S. Schmool, J. S. Garitaonandia, and J. M. Barandiarán, "Magnetic evolution of the amorphous and nanocrystalline phases and interphase coupling during the crystallization of $Fe_{87}Zr_6B_6Cu$: A ferromagnetic resonance study," *Phys. Rev. B, Condens. Matter*, vol. 58, pp. 12159–12168, Nov. 1998.

[17] M. W. Chen, A. Sakai, A. Inoue, X. M. Wang, Y. Watanabe, and T. Sakurai, "Partitioning behavior of Al in a nanocrystalline FeZrBAl soft magnetic alloy," *J. Appl. Phys.*, vol. 87, pp. 439–442, Dec. 2000.

[18] C. Herring and C. Kittel, "On the theory of spin waves in ferromagnetic media," *Phys. Rev. J. Arch.*, vol. 81, pp. 869–880, Mar. 1951.

[19] C. Kittel, "Interaction of spin waves and ultrasonic waves in ferromagnetic crystals," *Phys. Rev. J. Arch.*, vol. 110, pp. 836–841, May 1958.

[20] E. Schlömann, "Spin-wave analysis of ferromagnetic resonance in polycrystalline ferrites," *J. Phys. Chem. Solids*, vol. 6, pp. 242–256, Aug. 1958.

[21] R. Arias and D. L. Mills, "Extrinsic contributions to the ferromagnetic resonance response of ultrathin films," *Phys. Rev. B, Condens. Matter*, vol. 60, pp. 7395–7409, Sep. 1999.

[22] E. Schlömann, "Inhomogeneous broadening of ferromagnetic resonance lines," *J. Appl. Phys.*, vol. 40, pp. 1199–1201, Mar. 1969.

[23] R. A. Gallardo *et al.*, "Splitting of spin-wave modes in thin films with arrays of periodic perturbations: Theory and experiment," *New J. Phys.*, vol. 16, p. 023015, Feb. 2014.

[24] D. S. Schmool and J. M. Barandiarán, "Ferromagnetic resonance and spin wave resonance in multiphase materials: Theoretical considerations," *J. Phys., Condens. Matter*, vol. 10, no. 47, p. 10679, 1998.

[25] C. Kittel, "On the theory of ferromagnetic resonance absorption," *Phys. Rev. J. Arch.*, vol. 73, pp. 155–161, Jan. 1948.

[26] C. Kittel, "On the gyromagnetic ratio and spectroscopic splitting factor of ferromagnetic substances," *Phys. Rev. J. Arch.*, vol. 76, pp. 743–748, Sep. 1949.

[27] T. L. Gilbert, "A phenomenological theory of damping in ferromagnetic materials," *IEEE Trans. Magn.*, vol. 40, no. 6, pp. 3443–3449, Nov. 2004.
[28] R. D. McMichael and P. Krivosik, "Classical model of extrinsic ferromagnetic resonance linewidth in ultrathin films," *IEEE Trans. Magn.*, vol. 40, no. 1, pp. 2–11, Jan. 2004.
[29] Q. Zeng, I. Baker, V. McCreary, and Z. Yan, "Soft ferromagnetism in nanostructured mechanical alloying FeCo-based powders," *J. Magn. Magn. Mater.*, vol. 318, pp. 28–38, Nov. 2007.
[30] P. Scherrer, "Bestimmung der inneren Struktur und der Größe von Kolloidteilchen mittels Röntgenstrahlen," in *Kolloidchemie Ein Lehrbuch*, R. Zsigmondy, Ed. Berlin, Germany: Springer, 1912, pp. 387–409.
[31] A. L. Patterson, "The Scherrer formula for X-ray particle size determination," *Phys. Rev. J. Arch.*, vol. 56, pp. 978–982, Nov. 1939.
[32] K. J. Harte, "Theory of magnetization ripple in ferromagnetic films," *J. Appl. Phys.*, vol. 39, pp. 1503–1524, Feb. 1968.
[33] B. D. Cullity and C. D. Graham, "Domains and the magnetization process," in *Introduction to Magnetic Materials*. Hoboken, NJ, USA: Wiley, 2008, pp. 275–333.
[34] A. M. Clogston, H. Suhl, L. R. Walker, and P. W. Anderson, "Possible source of line width in ferromagnetic resonance," *Phys. Rev. J. Arch.*, vol. 101, pp. 903–905, Jan. 1956.
[35] A. M. Clogston, H. Suhl, L. R. Walker, and P. W. Anderson, "Ferromagnetic resonance line width in insulating materials," *J. Phys. Chem. Solids*, vol. 1, pp. 129–136, Nov. 1956.
[36] R. H. Victora, L. M. Falicov, and S. Ishida, "Calculated surface electronic structure of ferromagnetic iron and the ferromagnetic ordered iron-cobalt alloy," *Phys. Rev. B, Condens. Matter*, vol. 30, pp. 3896–3902, Oct. 1984.
[37] J. Pelzl, R. Meckenstock, D. Spoddig, F. Schreiber, J. Pflaum, and Z. Frait, "Spin–orbit-coupling effects on g-value and damping factor of the ferromagnetic resonance in Co and Fe films," *J. Phys.-Condens. Matter*, vol. 15, pp. S451–S463, Feb. 2003.
[38] B. Buford, P. Dhagat, and A. Jander, "A technique for error estimation of linewidth and damping parameters extracted from ferromagnetic resonance measurements," *J. Appl. Phys.*, vol. 117, p. 17E109, May 2015.
[39] M. P. R. Sabino, S. T. Lim, and M. Tran, "Influence of Ta insertions on the magnetic properties of MgO/CoFeB/MgO films probed by ferromagnetic resonance," *Appl. Phys. Express*, vol. 7, p. 093002, Sep. 2014.
[40] M. Ranjbar *et al.*, "CoFeB-based spin Hall nano-oscillators," *IEEE Magn. Lett.*, vol. 5, Nov. 2014, Art. no. 3000504.
[41] A. Okada, S. Kanai, M. Yamanouchi, S. Ikeda, F. Matsukura, and H. Ohno, "Electric-field effects on magnetic anisotropy and damping constant in Ta/CoFeB/MgO investigated by ferromagnetic resonance," *Appl. Phys. Lett.*, vol. 105, p. 052415, Aug. 2014.

Ryan A. O'Dell was born in Mansfield, OH, USA, in 1986. He received the B.S. degree in physics from Ashland University, Ashland, OH, USA, in 2010, the M.S. degree in physics from Bowling Green State University, Bowling Green, OH, USA, in 2013, and the Ph.D. degree in electrical engineering and computer science from The University of Toledo, Toledo, OH, USA, in 2018.

From 2010 to 2011, he was with the Charles River Research Laboratories, Ashland, OH, USA. He was with the Air Force Research Laboratory, Dayton, OH, USA, where he was involved in next-generation spintronic materials.

Dr. O'Dell is a member of the National Society of Black Engineers and SPIE. He was a recipient of the Dayton Area Graduate Studies Institute Ph.D. Fellowship from the Air Force Research Laboratoryin 2015.

Adam B. Phillips received the Ph.D. degree in physics from The University of Virginia, Charlottesville, VA, USA, in 2007.

Since 2008, he has been a Research Assistant Professor at The University of Toledo, Toledo, OH, USA, where he focuses on using carbon nanotubes (CNT) and CNT-hybrid materials in photovoltaics.

Daniel G. Georgiev (SM'12) received the Ph.D. degree in electrical engineering from the University of Cincinnati, Cincinnati, OH, USA, in 2003.

He was a Research Faculty at Wayne State University, Detroit, MI, USA. Since 2006, he has been with the Electrical Engineering and Computer Science Department, The University of Toledo, Toledo, OH, USA, where he is currently an Associate Professor.

John G. Jones received B.S. degree in electrical engineering from the Rose-Hulman Institute of Technology, Terre Haute, IN, USA, in 1991, and the Ph.D. degree from the University of Cincinnati, Cincinnati, OH, USA, in 1997.

He is a Senior Materials Research Engineer for the U.S. Air Force Research Laboratory, Nanoelectronics Materials Branch of the Materials and Manufacturing Directorate. His research interests include nanoelectronics thin-film materials process development utilizing PVD, *in situ* ellipsometry for closed-loop feedback, and engineering second-order nonlinear optical materials.

Gail J. Brown received the Ph.D. degree from the University of Dayton, Dayton, OH, USA, in 1994.

She was a Principal Physicist with the Nanoelectronics Materials Branch of the Materials and Manufacturing Directorate, Air Force Research Laboratory, from 1980 to 2017. She led a team of researchers involved in advanced electronic materials research, such as multiferroic materials for RF and microwave electronics, and semiconductor superlattices for infrared sensing. She is currently teaching physics at the University of Dayton.

Michael J. Heben received the Ph.D. degree in chemistry from the California Institute of Technology, Pasadena, CA, USA, in 1990.

He was a Principal Scientist for The National Renewable Energy Laboratory, Denver, CO, USA, from 1990 to 2008. Since 2008, he has been a Professor of physics and an Endowed Chair for Wright Center for Photovoltaic Innovations and Commercialization, The University of Toledo, Toledo, OH, USA.